Journal of Molecular Catalysis A: Chemical 380 (2013) 49–56

Contents lists available at ScienceDirect

Journal of Molecular Catalysis A: Chemical

journal homepage: www.elsevier.com/locate/molcata

Preparation of supported POM catalysts for liquid phase oxydehydration of glycerol to acrylic acid

Sarawalee Thanasilp[a], Johannes W. Schwank[b], Vissanu Meeyoo[c], Sitthiphong Pengpanich[c], Mali Hunsom[a,d,*]

[a] Fuels Research Center, Department of Chemical Technology, Faculty of Science, Chulalongkorn University, 254 Phayathai Road, Bangkok 10330, Thailand
[b] Department of Chemical Engineering, College of Engineering, University of Michigan, Ann Arbor, MI, USA
[c] Department of Chemical Engineering, Mahanakorn University of Technology, Bangkok, Thailand
[d] Center of Excellence on Petrochemical and Materials Technology (PETRO-MAT), Chulalongkorn University, 254 Phayathai Road, Bangkok 10330, Thailand

ARTICLE INFO

Article history:
Received 9 July 2013
Received in revised form
16 September 2013
Accepted 16 September 2013
Available online 23 September 2013

Keywords:
Glycerol
Oxydehydration
Polyoxometalate
Acrylic acid

ABSTRACT

A series of alumina-supported polyoxometalate (Al_2O_3-supported POM) catalysts was prepared by the impregnation method for the liquid phase catalytic oxydehydration of glycerol to acrylic acid in a batch reactor at low temperature (90 °C). The effect of types of polyoxometalate (POM) catalyst (PW, PMo, and SiW) and loading (2–8 wt.%) on the conversion and product yield was investigated. In the presence of Al_2O_3-supported POM catalyst, besides acrylic acid, various other higher market value products were generated, such as glycolic acid, propanediol, formic acid, acetic acid, and acrolein. The acid strength of Al_2O_3-supported POM catalysts played an importance role on the conversion and product yield of the oxydehydration of glycerol. Among the utilized Al_2O_3-supported POM catalysts, SiW/Al_2O_3 at 4 wt.% loading exhibited the highest glycerol conversion of about 84% with a yield of acrylic acid of around 25%.

1. Introduction

Glycerol is identified as one of the top biorefinery feed stocks in this decade [1]. Typically, it can be produced by either microbial fermentation [2], or by chemical synthesis from petrochemical feedstocks such as the oxidation or chlorination of propylene [3]. Also, it can be recovered as a by-product of either soap production by saponification or biodiesel production by transesterification of triglycerides from vegetable oils or animal fats [4]. Approximately 100 kg of glycerol is generated when a ton of biodiesel is produced. Any further increase in biodiesel production rates will significantly raise the quantity of glycerol above the demands and so decrease its economic value. Therefore, using the growing supply of glycerol is a logical step in moving toward a more sustainable economy. In order to find new uses of glycerol, for making biodiesel production more cost effective, various previous research efforts have focused on transforming glycerol into more valuable chemicals such as propanediol [5–10], synthesis gas [11–15], acrylonitrile [16,17], or liquid fuels [18–21].

Acrylic acid is one of the most interesting and important chemicals that is widely used in adhesive, paint, plastic, and rubber synthesis. Typically, acrylic acid can be produced by the oxidation of acrolein over various types of mixed oxide catalysts [22–25]. It can also be produced from glycerol via a two-step reaction process including dehydration of glycerol into acrolein and oxidation of acrolein into acrylic acid by either using a single bifunctional catalyst via the one-pot approach or by using a process that involves two separate steps [16]. For the one-pot approach, the iron oxide (FeO_x) domains on the surface of an iron orthovanadate ($FeVO_4$) phase exhibited a better catalytic activity for the oxidative dehydration than FeO_x catalyst prepared by impregnation and a mixture of $FeVO_4$ and Fe_2O_3 [26]. High acrylic acid yields up to 14% were obtained in a fixed-bed reactor at 300 °C with a feed composition N_2:O_2:H_2O:glycerol = 66.6:1.7:30.3:1.5. The hemihydrate $VOHPO_4$ $0.5H_2O$ oxide emerged as the best catalyst for complete dehydration of glycerol at 300 °C in a gas-phase fixed-bed reactor [27]. The addition of oxygen helped maintain an oxidized state of the catalyst and eliminated coke formation [28]. However, this catalyst was less active toward the one-step conversion of glycerol to acrylic acid due to its low oxidation ability. In gas phase reaction at 300 °C over MoVTeNbO catalysts, almost complete conversion of glycerol (99.6%) was achieved with a high yield of acrylic acid (28.4%) [29]. However, this was accompanied by a high yield (up to 23%) of undesired acetic acid byproduct. W—V—O bronze catalysts

* Corresponding author at: Fuels Research Center, Department of Chemical Technology, Faculty of Science, Chulalongkorn University, 254 Phayathai Road, Bangkok 10330, Thailand. Tel.: +66 2 2187523 5; fax: +66 2 2555831.
E-mail address: mali.h@chula.ac.th (M. Hunsom).

1381-1169/$ – see front matter © 2013 Elsevier B.V. All rights reserved.
http://dx.doi.org/10.1016/j.molcata.2013.09.023

with hexagonal tungsten bronze (HBT) structure and a V/(W + V) ratio in the range of 0.12–0.21 allowed the consecutive one-pot oxidation of acrolein into acrylic acid with up to 25% yield [30]. High acrylic acid yield up to 34% was obtained at 290 °C by incorporation of Nb^{5+} into the tri-component bronze structure (W—V—Nb) with atomic ratios V/(W + V + Nb) = 0.13 and Nb/(W + V + Nb) = 0.13 [16]. To increase acrylic acid yield, a two-bed system was used to convert glycerol to acrolein over azeolite catalyst followed by selective oxidation of acrolein to acrylic acid over a V—Mo oxide catalyst [31]. Complete conversion of 10–30 wt.% glycerol with high selectivity to acrolein up to 81 mol% was achieved with medium pore zeolites (HZSM-5) at 300 °C. A separated-sequential bed system provided high selectivity for acrylic acid up to 98% but low acrolein conversion of 48%. Although this system can maximize the acrylic acid yield and avoid the oxidation of glycerol in the second bed, the oxidation of acrolein to acrylic acid required high catalyst loading up to 48 wt.%, resulting in the agglomeration of the mixed oxide phase. In addition, the presence of high vanadium content in the second reactor can promote the decomposition/evolution of the "surface pools" into small oxygenates such as acetaldehyde, acetol, acetic acid, and coke deposits that readily leads to catalyst deactivation [31].

In the present work, Al_2O_3-supported POM catalysts are used in a one-pot process for the liquid phase conversion of glycerol to acrylic acid, with the goal to simplify the process and reduce the capital cost of the process. The influence of catalyst types, catalyst loadings, and reaction time on glycerol conversion and product yields is investigated. Finally, a reaction pathway of glycerol oxydehydration in the presence of Al_2O_3-supported POM catalysts is proposed.

2. Experimental

2.1. Catalyst preparation and characterization

Three types of commercial polyoxometalate (POM) including phosphomolybdic acid ($H_3PMo_{12}O_{40}{\cdot}xH_2O$, PMo), phosphotungstic acid ($H_3PW_{12}O_{40}{\cdot}xH_2O$, PW), and silicotungstic acid ($H_4SiW_{12}O_{40}{\cdot}xH_2O$, SiW) were impregnated on commercial Al_2O_3 (pore diameter of 5.8 nm; Sigma–Aldrich® INC.) by the incipient wetness impregnation method at constant POM loading of 30 wt.%. Initially, 2.14 g of POM was dissolved thoroughly in 5 ml distilled water at room temperature. Then, approximately 5 g of Al_2O_3 was added slowly into this solution. The obtained slurry was stirred at constant rate of 200 rpm at room temperature for 1 h. The ready-to-use supported POM catalysts were obtained after drying at 110 °C for 20 h followed by calcination at 400 °C for 4 h. The BET surface area, pore volume, and average pore diameter for fresh solids were derived from nitrogen adsorption isotherms measured at −196 °C (Micromeritics ASAP 2020). Prior the measurement, each sample was degassed at 200 °C for 4 h. The average pore diameters were calculated according to BJH method. The phase structures of the catalysts were determined based on powder X-ray diffraction patterns (XRD) on a Siemens PE-2004 X-ray diffractometer using Cu $K\alpha$ (λ = 0.15406 nm) radiation operated at 40 kV and 20 mA. The local interactions in PW/Al_2O_3 and PMo/Al_2O_3 were determined by ^{31}P MAS NMR spectra on a Varian INOVA-500 MHz spectrometer with CP/MAS solid-probe and nano-probe with the Larmor frequencies of ^{1}H and ^{31}P at 500.16 MHz and 202.46 MHz, respectively. The local interaction in SiW/Al_2O_3 was probed by ^{29}Si MAS NMR spectra on a Varian INOVA-500 MHz spectrometer with CP/MAS solid-probe and nano-probe with the Larmor frequencies of ^{1}H and ^{29}Si at 500.15 MHz and 99.36 MHz, respectively. The acidities of all supported POM catalysts were determined by temperature-programmed desorption of ammonia (NH_3-TPD) in a fixed-bed continuous flow microreactor at atmospheric pressure equipped with TCD detector. 50 mg of catalysts were pretreated at 200 °C for 60 min under He flow. After cooling down to room temperature under He flow, NH_3 chemisorption was carried out by passing He at a flow rate of 30 ml/min first through a saturator containing NH_4OH solution at room temperature, then through a moisture trap. The NH_3-saturated He stream was then passed through the catalyst bed for 30 min at room temperature. Finally, the reactor was purged with pure He flow at room temperature for 30 min. The catalysts were then heated under He flow (30 ml/min) up to 700 °C with a linear heating rate of 10 °C/min, and the temperature-programmed desorption of NH_3 was measured using a TCD detector.

To determine the amount of oxygen adsorbed/desorbed on the surface of the supported POM catalysts, the temperature-programmed desorption of oxygen (O_2-TPD) was carried out in fixed-bed continuous flow microreactor at atmospheric pressure equipped with TCD detector, using 5% O_2 in He at various adsorption temperatures. Prior to desorption, the O_2/He flow was passed with a flow rate of 30 ml/min through the catalyst bed at 200 °C for 60 min. The catalysts were then heated under He flow (30 ml/min) up to 1000 °C with a linear heating rate of 10 °C/min. The structural integrity of the Keggin units in supported POM catalysts was characterized by Fourier transform infrared (FT-IR) spectroscopy, recorded on a Perkin Elmer Spectrum One instrument.

2.2. Catalytic activity test

Catalytic oxydehydration of glycerol to acrylic acid was carried out in a liquid phase batch reactor system at 90 °C and ambient pressure. The mole ratio of glycerol and H_2O_2 was fixed at 1:2. Initially, 30 ml of 20 wt.% aqueous glycerol solution (99.5% (v/v), Fisher) was mixed with the desired quantity of supported POM catalyst (0.15 g, 0.30 g, and 0.60 g or 2 wt.%, 4 wt.%, and 8 wt.%, respectively) in a 500 ml three-neck round bottom flask equipped with a reflux condenser and stirrer. The temperature of the system was raised to 90 °C by an external electrical heater. When the required temperature was reached, 12.72 ml H_2O_2 (Fisher) was added slowly. The reaction was monitored by taking liquid samples of about 1.0 ml at regular time intervals until 4 h of reaction time had elapsed. To terminate the reaction, the liquid product samples were quenched in an ice-water trap at a temperature of 0–5 °C and then centrifuged on a Hermle Z206A Digital Laboratory Centrifuge to separate the solid catalyst from the aqueous product. To identify all generated products, a GC–MS (GC 7890A/MS 5975C, Agilent technologies) equipped with DBwax capillary column was used. The quantities of the desired products including glycolic acid, formic acid, acetic acid, acrolein and acrylic acid were quantitatively analyzed by high performance liquid chromatography (HPLC, Waters 410 HPLC controller) equipped with a refractive index detector in series. A Phenomenex Luna 5 μm C18 (2) 100 (25 cm × 4.6 mm) was used as separating HPLC column.

3. Results and discussion

3.1. Properties of fresh supported POM catalyst

Textural properties for supported POM catalyst immobilized on Al_2O_3 support derived from nitrogen physisorption isotherms are summarized in Table 1. The BET surface area, pore volume as well average pore diameter of all Al_2O_3-supported POM decreased significantly compared to the original POM-free supports. The decrease in BET surface area may be attributed to the support pores blocking by active POM. This is because the pores of Al_2O_3 are 5.46 Å and the Keggin unit diameter is ~12 Å [32]. Thus, it is reasonable to conclude that the pores are blocked by the active phase.

Table 1
Textural properties of Al_2O_3 and Al_2O_3-supported POM.

Catalysts	BET surface area (m^2/g)	Pore volume (cm^3/g)	Average pore diameter (Å)
Al_2O_3	267.8	0.229	5.46
PW/Al_2O_3	227.4	0.156	4.53
PMo/Al_2O_3	221.5	0.143	4.26
SiW/Al_2O_3	214.6	0.128	4.11

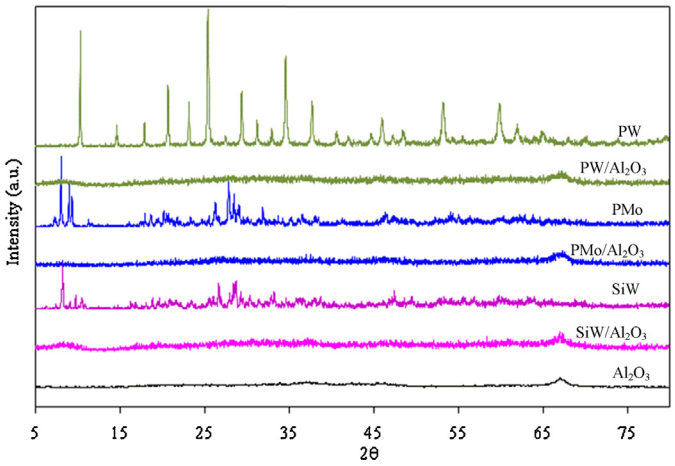

Fig. 1. XRD patterns of Al_2O_3, POM catalysts and Al_2O_3-supported POM catalysts at 30 wt.% POM loading.

Prior to testing the activity of supported POM catalysts, their identities and characteristics of as-prepared catalysts were first characterized. As shown in Fig. 1, the XRD pattern of Al_2O_3 was amorphous and showed no crystalline phase. Among the non-supported POM catalysts, the PW catalyst demonstrated the sharp peaks of Keggin-type PW phase at 2θ of 10.3 and 25.3 (PDF 75-2125). The PMo revealed the characteristic peaks at 2θ of 27.3 and 23.3, indicating the presence of MoO_3 phase (PDF 89-7112). For SiW, the XRD pattern showed the peaks at 2θ of 27.3°, assigned to the SiW hexahydrate [34]. However, for Al_2O_3-supported POMs, the patterns resembled that of Al_2O_3 and no characteristic peaks assignable to the utilized POMs were observed, suggesting that the POM catalysts were highly dispersed on the alumina surface.

To confirm the presence of the Keggin anions on the Al_2O_3 surface, FT-IR spectra were recorded (Fig. 2). The blank Al_2O_3 displayed the broad absorption bands at 3300–3700 cm^{-1} and at around

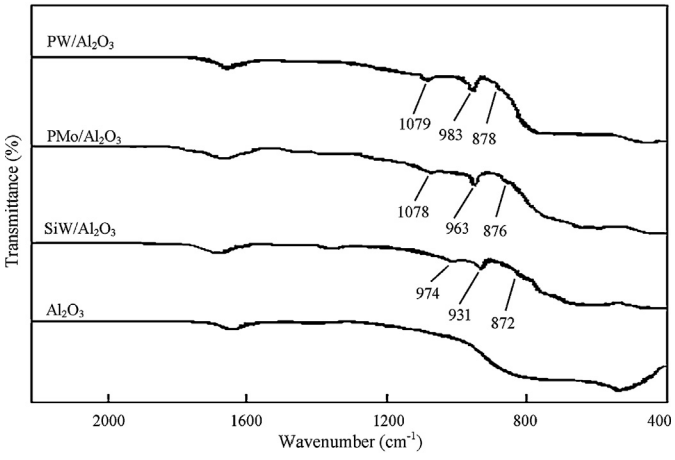

Fig. 2. FT-IR spectra of Al_2O_3 and Al_2O_3-supported POM catalysts at 30 wt.% POM loading.

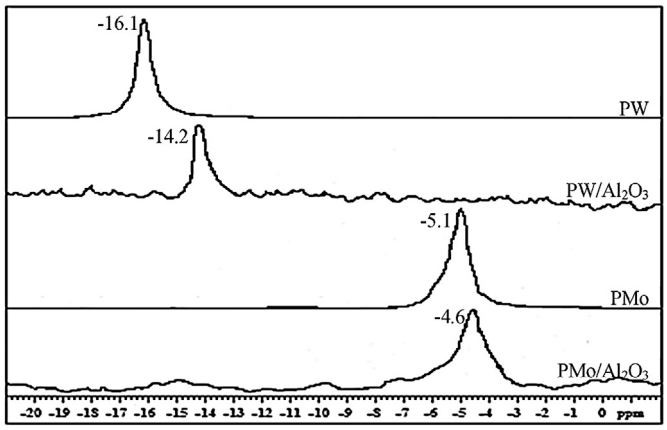

Fig. 3. ^{31}P MAS NMR spectra of PW/Al_2O_3 and PMo/Al_2O_3 catalysts at 30 wt.% POM loading.

1650 cm^{-1}, assigned to hydroxyl group O—H vibration. The broad overlapping peaks in the lower frequency range (500–1000 cm^{-1}) were due to the presence of Al—O (780 and 690 cm^{-1}) infrared vibrations. For supported POM catalysts, besides the main characteristic peaks of Al_2O_3, additional peaks were observed. The polyanions ($PW_{12}O_{40}^{3-}$) consisted of a PO_4 tetrahedron surrounded by four W_3O_{13} groups formed by edge-sharing octahedral was observed for PW. These groups are connected to each other by corner-sharing oxygens [33], and this arrangement gives rise to four types of bands between 1200 and 700 cm^{-1}. The bands observed at 1079 cm^{-1}, 983 cm^{-1} and 878 cm^{-1} are related to the asymmetric stretching of P—O, asymmetric stretching of terminal oxygen (W=O_t) and asymmetric stretching of center oxygen (W—O_c—W), respectively. Also, a shoulder peak a wave number 797 cm^{-1} can be assigned to the asymmetric stretching of edge oxygen (W—O_e—W) [35,36]. For PMo/Al_2O_3, the main characteristic bands of the Keggin units at 1078 and 963 cm^{-1} were assigned to the asymmetric stretching of P—O and center oxygen (Mo—O_c—Mo), respectively. The weak shoulders at 876 and 785 cm^{-1} were related to the symmetric stretching of terminal oxygen (Mo—O_t) and edge oxygen (Mo—O_e—Mo), respectively [37,38]. For SiW/Al_2O_3, the parent $[SiW_{12}O_{40}]^{4-}$ Keggin structure displayed the characteristic bands due to W—O—W vibrations of edge- and corner-sharing WO_6 octahedra linked to the central SiO_4 tetrahedral [39,40]. As demonstrated in Fig. 2, the stretching modes of edge sharing (W—O_e—W) and center sharing (W—O_c—W) units emerged as shoulders at 793 and 872 cm^{-1}, respectively, whereas the Si—O stretching modes appeared at 931 and 974 cm^{-1}. According to the obtained FT-IR results, it can be confirmed that the POMs supported on Al_2O_3 retained their Keggin structures under our preparation procedure.

In order to examine the local interactions and structural changes in PW/Al_2O_3 and PMo/Al_2O_3 catalysts and its support, ^{31}P MAS NMR spectroscopy was utilized (Fig. 3). For unsupported PW, a single symmetry narrow peak was observed at −16.1 ppm, indicating the presence of PW in hexahydrated form. The $PW_{12}O_{40}^{3-}$ anions in the hexahydrate are packed in a cubic structure and all acidic protons are presented in the form of $H_5O_2^+$ cations [41]. In the case of PW/Al_2O_3, a down field shift of the peak to −14.2 ppm was observed. This might be attributed to the partial loss of some water molecules from the PW crystallites during the immobilization of PW onto the Al_2O_3 support during impregnation [42]. In addition, the down field chemical shift of the peak in ^{31}P MAS NMR spectrum indicated the interaction of PW with the Al_2O_3 support. This shift behavior was also observed during the immobilization of PW onto another support such as SiO_2 [41,43,44]. The fact that single peaks were observed in the NMR spectra for both PW and PW/Al_2O_3,

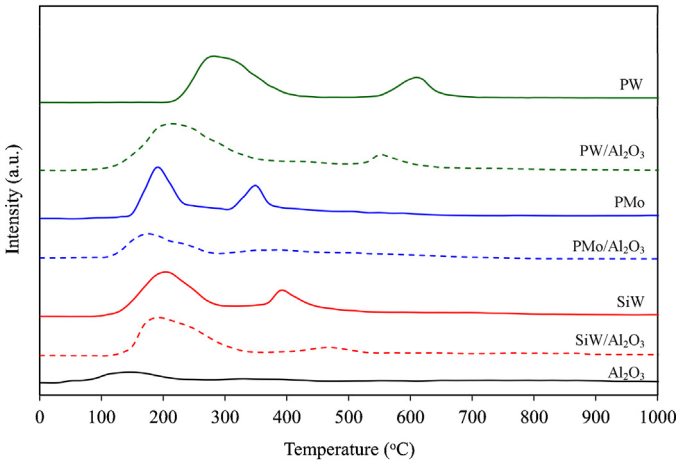

Fig. 4. NH_3-TPD profiles of POM catalyst and Al_2O_3-supported-POM catalysts at 30 wt.% POM loading.

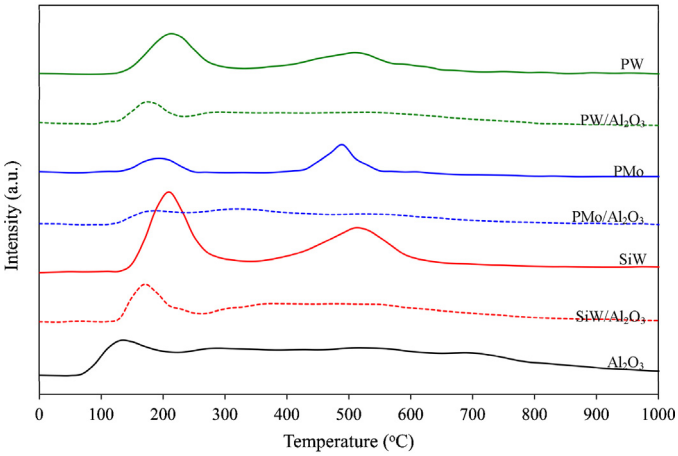

Fig. 5. O_2-TPD profiles of POM catalysts and Al_2O_3-supported-POM catalysts at 30 wt.% POM loading.

suggests the uniformity and high symmetry of the crystal structure in which all polyanions are equally hydrogen bonded by $H_5O_2^+$ cations. In the case of PMo, the fresh unsupported PMo exhibited an almost symmetric resonance peak at a chemical shift of −5.1 ppm, indicating the presence of phosphorous in the tetrahedral position of the Keggin structure [45] or a uniform phosphorus environment in the highly hydrated structure of PMo [46]. A smaller shoulder peak close to the main peak at a chemical shift of −4.6 ppm was attributed to a non-uniform hydration of the sample [47]. The ^{31}P NMR spectrum of PMo/Al_2O_3 shifted considerably toward lower field at a chemical shift of −4.6 ppm, caused by loss of water as well as the interaction between the Keggin unit and the Al_2O_3 support [45]. For investigating the local interaction and structural changes in the SiW/Al_2O_3 catalyst, ^{29}Si MAS NMR spectroscopy was utilized instead. No peaks assigned to the main characteristics of SiW in the NMR spectrum of either SiW or SiW/Al_2O_3. In the case of ^{29}Si NMR spectroscopy, low isotopic abundance, a small, negative magnetogyric ratio, and long relaxation times contribute to experimental difficulty [48].

The surface acidity of the utilized POMs and the supported POM catalysts was determined by NH_3-TPD analysis as shown in Fig. 4. Theoretically, acid sites can be classified as weak- (150–300 °C), medium- (300–500 °C) and strong- (500–650 °C) strength [49]. For PW, two broad NH_3-TPD peaks appearing at the temperatures of 280 and 610 °C indicated the presence of medium- and strong-strength acid sites. On the supported PW/Al_2O_3 sample, both peaks shifted to lower temperatures and lost some intensity, indicating a weakening of the acid sites due to interactions with the alumina support. For PMo, peaks assigned to weak- and medium-strength acid sites appeared at 189 and 352 °C. On the supported PMo/Al_2O_3 sample, the peaks shifted to slightly lower temperatures and lost considerable intensity, again indicating loss of acid strength due to interactions with the support. SiW gave peaks at 203 and 388 °C. Upon supporting SiW on Al_2O_3, the medium strength peak lost most of its intensity but appeared to shift toward higher temperature (~475 °C).

As summarized in Table 2, the total acidity of the POM catalysts was in an order of PW > SiW > PMo, consistent with that reported by Shen et al. [17]. When POMs were impregnated on the surface of Al_2O_3, the intensity of TPD peaks was reduced and shifted to low temperature indicating the decrease in acid concentration and acidity strength of Al_2O_3-supported POM catalysts. However, the acidities of the POM catalysts were still greater than that of pure Al_2O_3. Atia et al. suggested that the addition of POM did not introduce any new acid sites on support surface, but led to a replacement by other acidic sites [49]. The weak interaction of Al_2O_3 with the POM kept its Brønsted acid character and led to an increased proportion of medium- and strong-strength acid sites. In this case, a portion of the POM would loosen its acidity due to the distortion of the Keggin structure.

The O_2-TPD spectra of the unsupported POM catalysts and Al_2O_3-supported POM catalysts after O_2 adsorption at different temperatures are shown in Fig. 5 and Table 3. The results show that both POM and Al_2O_3-supported POM catalysts have the ability to adsorb and desorb O_2. The total O_2 desorption of the POM catalysts was in an order of SiW > PW > PMo, suggesting that the SiW demonstrated the highest reducibility or oxidative ability. When POMs were impregnated on the surface of Al_2O_3, a similar trend of oxidative ability was still observed. That is, the total O_2 desorption was in the order of $SiW/Al_2O_3 > PW/Al_2O_3 > PMo/Al_2O_3$. Nevertheless, the quantities of the total O_2 desorption were reduced, indicating the decrease in adsorption/desorption strength of Al_2O_3-supported POM catalysts.

3.2. Catalytic activity test

3.2.1. Preliminary activity test

The initial activity tests of catalytic oxydehydration of glycerol were carried out in a batch reactor at a temperature of 90 °C at ambient pressure in the presence of 2 wt.% Al_2O_3-supported POM catalysts at reaction times of 2 h. As clearly demonstrated in the GC–MS spectra (Fig. S.1), besides the preferable compound (acrylic acid), several other products were detected in the GC–MS chromatogram. In the presence of all Al_2O_3-supported POM catalysts, C_1—C_3 oxygenated products (formic acid, acetic acid, hydroxyacetic acid or glycolic acid, acrolein, and acrylic acid) as well as higher cyclic molecules (5-hydroxy-1,3-dioxolane, 5-hydroxyl-2-methyl-1,3-dioxane, benzoic acid) were generated. In addition, some oxygenated products including 1-hydroxyl-2-propanone or acetol, propanoic acid, 2,3-dihydroxyl-propanal and hydroxyacetic acid (glycolic acid) were found in the presence of either PW/Al_2O_3 or SiW/Al_2O_3, while 2-ethoxyethanol was observed in the presence of SiW/Al_2O_3.

Supplementary material related to this article can be found, in the online version, at http://dx.doi.org/10.1016/j.molcata.2013.09.023.

3.2.2. Effect of parameters on catalytic oxydehydration of glycerol

Fig. 6 shows the conversion and desired product yields as a function of time in the presence of all the Al_2O_3-supported POM catalysts at 4 wt.% catalyst loading, 90 °C, and ambient pressure

Table 2
NH_3-TPD results for Al_2O_3, POM catalysts and Al_2O_3-supported POM catalysts.

Catalysts	NH_3-TPD peak position (°C)	Acid amount (mmol NH_3/g Cat.)	Total acidity (mmol NH_3/g Cat.) (measurable)	Total acidity[a] (mmol NH_3/g Cat.) (theoretical)
PW	280	3.73 (204–445 °C)	4.92	–
	610	1.19 (540–664 °C)		
PMo	189	2.28 (151–257 °C)	3.14	–
	352	0.88 (311–410 °C)		
SiW	203	2.88 (108–303 °C)	3.81	–
	391	0.93 (351–439 °C)		
PW/Al_2O_3	214	1.24 (62–370 °C)	1.51	1.95
	550	0.27 (510–641 °C)		
PMo/Al_2O_3	176	0.66 (101–290 °C)	0.86	1.42
	387	0.20 (297–501 °C)		
SiW/Al_2O_3	191	1.19 (110–356 °C)	1.42	1.62
	469	0.23 (390–543 °C)		
Al_2O_3	151	0.50 (46–275 °C)	0.68	–
	330	0.18 (275–453 °C)		

[a] 30 wt.% the different POM catalysts of support.

in the presence of 2.74 M H_2O_2 with glycerol concentration of 20 wt.%. Glycerol conversion increased initially with the increasing reaction time and then leveled off at reaction times longer than 120 min. With regards to the variation of product yield, the yields of acetic acid, glycolic acid and formic acid increased with increasing reaction time. The yield of acrylic acid was low during the first 90–120 min of reaction time, while a high yield of acrolein was obtained during the same period. However, at longer reaction times, the yield of acrolein decreased, whilst the yield of acrylic acid increased. This implies that acrolein was oxidized to acrylic acid in the presence of Al_2O_3-supported POM catalysts [24,25].

Table 4 summarizes the glycerol conversion as well as the yield of desired products at 240 min of reaction time in the presence of different types and loadings of Al_2O_3-supported POM catalysts. Approximately 9.3% of glycerol can be converted in the absence of catalysts (blank test). The carbon balance (C balance) reported as the percentage of carbon accounted for the system (only the desired liquid products) at the end of 240 min was approximately 22%. The difference in mass balance is expected for the conversion of carbon atom in glycerol molecule to undesired products (both in gas and liquid phases) such as acetaldehyde, propanal, propanoic acid, propane-1,2-diol, propane-1,3-diol, 5-hydroxy-1,3-dioxolane, 5-hydroxyl-2-methyl-1,3-dioxane, benzoic acid as well as CO_2. In the presence of solely Al_2O_3, the conversion of glycerol increased significantly. The glycerol conversion nearly doubled as the Al_2O_3 loading was increased from 2 to 4 wt.%. This might be attributed to the presence of acid sites on the Al_2O_3 surface, enhancing the dehydration of glycerol to other substances. However, further raising the Al_2O_3 loading from 4 to 8 wt.% resulted in only a slight further increase of glycerol conversion, most likely due to mass transfer effects or limited availability of H_2O_2 in the system. Approximately 40–42% of converted carbons were transformed to the desired products. In the presence of Al_2O_3-supported POM catalysts, the glycerol conversion was greater than that in the presence of solely Al_2O_3 for all catalyst types and loadings. This is because the Al_2O_3-supported POM catalysts had more opportunity

Table 3
O_2-TPD results for Al_2O_3, POM catalysts and Al_2O_3-supported POM catalysts.

Types of catalyst	O_2-TPD peak position (°C)	O_2 desorption (mmol O_2/g Cat.)	Total O_2 desorption (mmol O_2/g Cat.)
PW	220	0.084 (104–319 °C)	0.123
	534	0.039 (386–650 °C)	
PMo	153	0.031 (145–256 °C)	0.090
	482	0.059 (397–549 °C)	
SiW	226	0.096 (124–313 °C)	0.185
	523	0.090 (365–669 °C)	
PW/Al_2O_3	174	0.039 (101–147 °C)	0.075
	539	0.037 (404–678 °C)	
PMo/Al_2O_3	181	0.024 (119–148 °C)	0.047
	325	0.015 (158–401 °C)	
	548	0.007 (454–667 °C)	
SiW/Al_2O_3	159	0.066 (119–275 °C)	0.102
	379	0.023 (281–479 °C)	
	508	0.013 (488–525 °C)	
Al_2O_3	139	0.063 (68–221 °C)	0.079
	298	0.006 (213–398 °C)	
	707	0.009 (649–851 °C)	

Table 4
Effect of catalyst types and loadings on the performance of glycerol oxydehydration over Al_2O_3-supported POM catalyst at temperature 90 °C and 240 min.

Types of catalyst	Loading (wt.%)	Glycerol conversion (%)	Carbon balance (%)[b]	Product yield (%)				
				Glycolic acid	Formic acid	Acetic acid	Acrolein	Acrylic acid
Blank[a]	–	9.27	22.21	0.29	0.52	0.55	0.16	0.67
Al_2O_3	2	36.94	40.30	3.50	1.23	4.69	1.15	4.31
	4	63.51	42.49	6.64	3.40	7.29	2.08	7.59
	8	65.69	40.01	6.53	3.20	7.18	1.92	7.46
PW/Al_2O_3	2	44.10	80.20	8.95	4.42	13.79	1.09	9.60
	4	72.93	86.26	15.07	9.17	23.19	3.48	16.20
	8	74.34	82.40	14.77	8.82	22.44	2.92	15.90
PMo/Al_2O_3	2	43.52	89.10	6.76	5.24	14.93	0.66	3.17
	4	66.62	87.40	13.07	10.32	31.10	1.28	6.30
	8	67.88	85.81	12.43	10.22	30.43	1.49	6.25
SiW/Al_2O_3	2	47.19	80.75	7.80	4.31	11.72	2.27	12.01
	4	83.78	80.02	15.34	7.90	18.83	5.44	25.11
	8	83.19	83.56	14.23	7.38	18.13	4.80	24.96

[a] Reaction at 90 °C for 240 min in the presence of only 2.74 M H_2O_2.
[b] Percent of carbon accounted after 240 min of reaction.

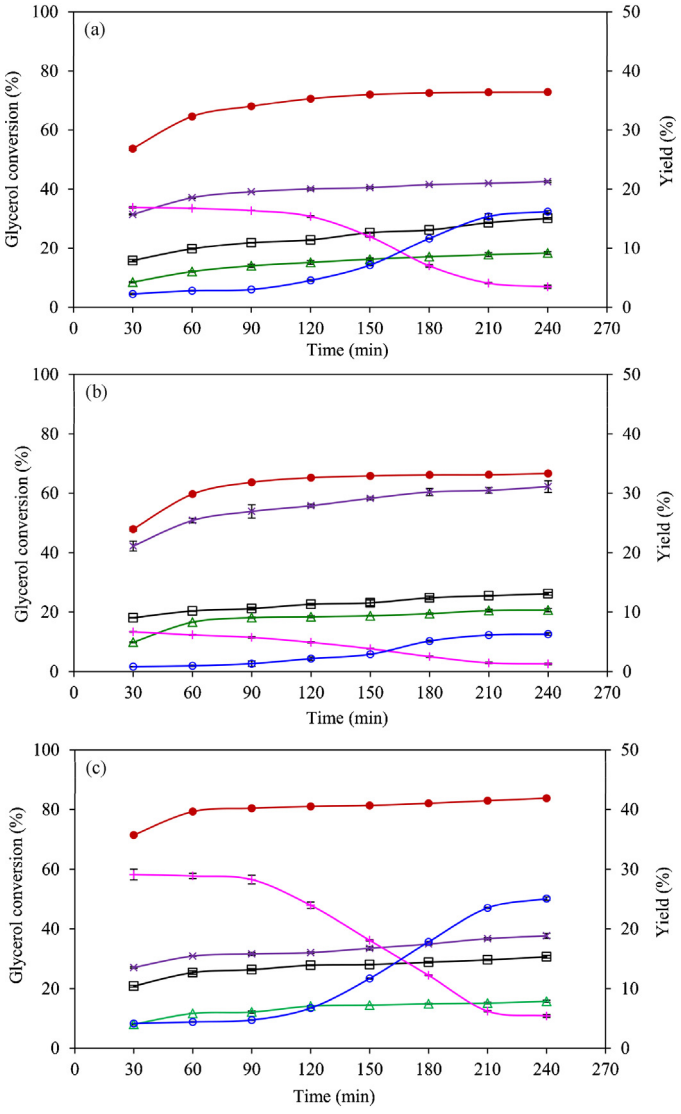

Fig. 6. Variation of (●) glycerol conversion and yields of (□) glycolic acid, (△) formic acid, (×) acetic acid, (+) acrolein and (○) acrylic acid as a function of time of glycerol oxydehydration over (a) PW/Al_2O_3, (b) PMo/Al_2O_3 and (c) SiW/Al_2O_3 at 90 °C and 4 wt.% catalyst loading.

to dehydrate glycerol due to their higher acid strengths compared with Al_2O_3 (Table 2). The glycerol conversion increased significantly as the catalyst loading doubled from 2 to 4 wt.%. Further increase of the catalyst loading up to 8 wt.% resulted again in only a slight further increase of glycerol conversion similarly to the trend of glycerol conversion in the presence of high Al_2O_3 loading. Although SiW/Al_2O_3 had lower acid strength than PW/Al_2O_3, it gave higher glycerol conversion under the same operating conditions. This could be due to the fact that SiW has better stability than PW under high reaction temperatures in aqueous media [33], resulting in a better chance to supply strong acid protons for the dehydration reaction of glycerol. PMo/Al_2O_3 had the lowest glycerol conversion compared with other utilized catalysts due to its low acid strength and thermal stability [50]. The carbon balance is attained more than 80% in each run, indicating that less than 20% of carbon was converted to undesired products.

With regard to the product yield of catalytic oxydehydration of glycerol, in the blank experiment less than 0.7% of each of the measurable detected products was formed (Table 4). When 2 wt.% Al_2O_3 was added, the yields of glycolic acid, acetic acid and acrolein increased significantly. Increasing the Al_2O_3 loading from 2 to 4 wt.% resulted in a yield increase of nearly a factor of two. Further increasing the Al_2O_3 loading to 8 wt.% led to a slight decrease of all desired products and an increase of other products. In the presence of Al_2O_3-supported POM catalysts, the yield of all desirable products increased considerably when the catalyst loading was increased from 2 to 4 wt.% but the yield decreased somewhat when the catalyst loading was further increased to 8 wt.%, similar to the change of product yield observed in the presence of solely Al_2O_3. One possible explanation is that at high catalyst loading the larger number of acidic sites or higher oxidative ability accelerates the oxydehydration of glycerol to other undesired products. However, it is also possible that this decrease in yield of desired products at high catalyst loading is due to the low mass transfer rate of reactants to the catalysts surface or the lack of sufficient oxidizing agent (H_2O_2). This hypothesis was already tested by increasing the amount of H_2O_2 from 2.74 M to 6.85 M. In the presence of 4 wt.% SiW/Al_2O_3 catalyst, the conversion of glycerol increased from 83.78% to 93.78% while the yield of acrolein decreased from 5.44 to 2.79% and the yield of acrylic acid from 25.11 to 17.86%. However, the presence of such high concentrations of H_2O_2 could lead to dangerous reaction conditions. Therefore, for safety reasons, the reaction was carried out with 2.74 M H_2O_2. Table 3 also shows that high quantities of acetic acid are generated in the presence of all Al_2O_3-supported POM catalysts, in the order of $PMo/Al_2O_3 > PW/Al_2O_3 > SiW/Al_2O_3$, in reverse order to their oxidative ability. Among the catalysts investigated, the

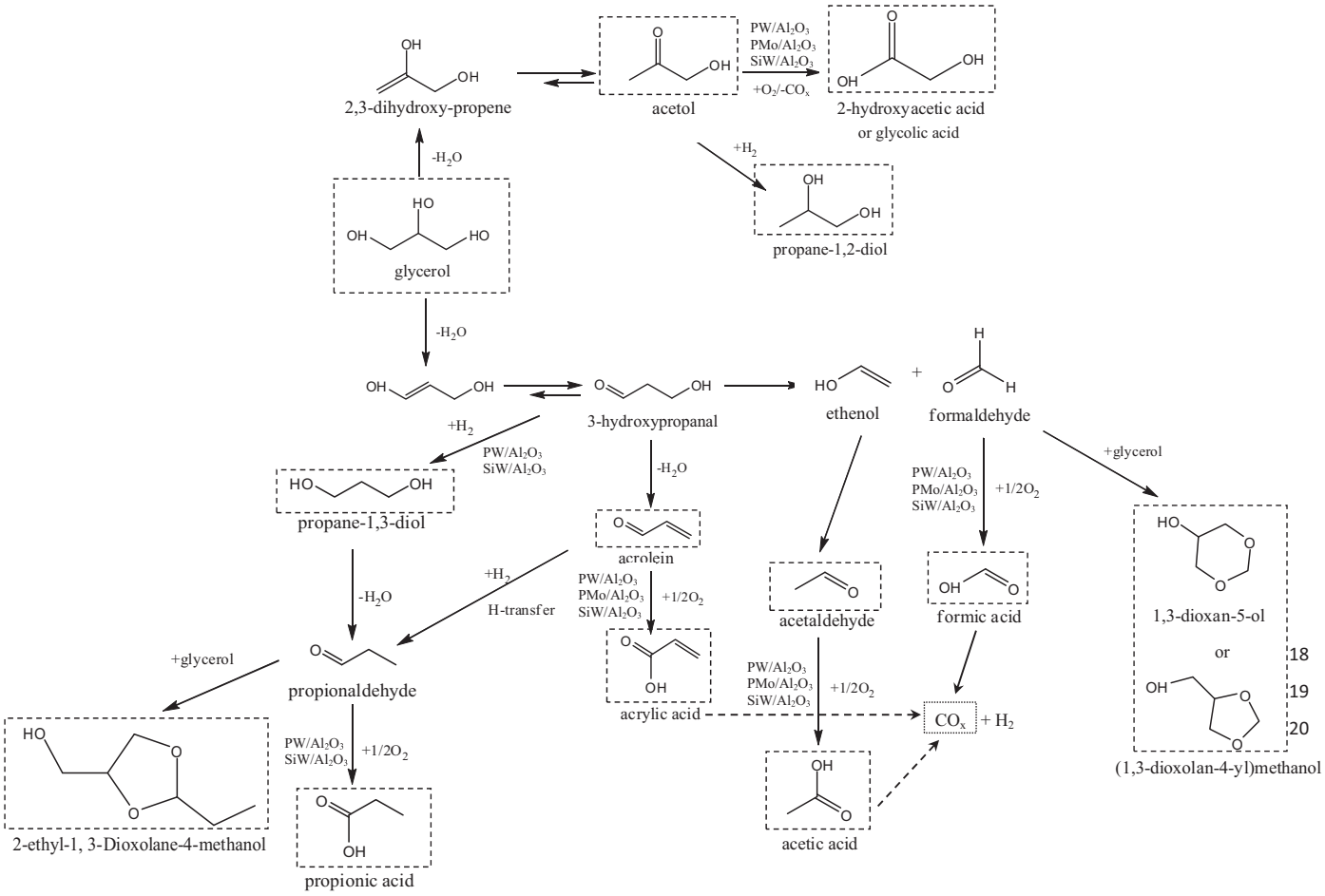

Scheme 1. Proposed reaction pathways of oxydehydration of glycerol. The products detected by GC–MS are indicated by dashed lines.

SiW/Al_2O_3 catalyst gave the highest production yield of acrylic acid of around 25.1% at a catalyst loading of 4 wt.%, thanks to its mild acidity and high oxidative ability.

3.2.3. *Reaction mechanism of oxydehydration of glycerol*

As detected by GC–MS chromatogram, a large number of compounds were generated in the catalytic oxydehydration of glycerol via Al_2O_3-supported POM catalysts at low temperature in liquid phase. Compared to glycerol, all of these formed compounds have many hydrogen and oxygen substitutions with C_2–C_6 carbon compounds being principally formed. While some of these compounds have known reaction pathways from glycerol, others do not. To optimize or standardize the oxydehydration of glycerol over the Al_2O_3-supported POM catalyst, it is important to know, and so to evaluate, the mechanisms of synthesis of these compounds from glycerol. However, it is still difficult to deduce the exact synthesis route of each compound from glycerol because some intermediate products cannot measure. Rather, a hypothetical general scheme (Scheme 1) can be proposed with some paths more or less possible for each studied system. According to this scheme, in the presence of Al_2O_3-supported POM catalysts, the dehydration of glycerol can occur both at the terminal and at the middle (or secondary) —OH groups. If glycerol is dehydrated at the terminal —OH group, 2,3-dihydroxypropene is generated. It can further rearrange to 1-hydroxyl-2-propanone or acetol, the detected product [51]. The acetol is very reactive, it is hydrogenated in the presence of acid catalysts to 1,2-propanediol, a commercially valuable chemical. Besides, acetol can be oxidized and decarboxylated to glycolic acid according to selective oxidation reaction and decarboxylation [52]. On the contrary, if glycerol was dehydrated at the second —OH group, H_2O and H^+ are extruded from the dehydrated glycerol to form two species; either 1,3-dihydroxypropene or 3-hydroxypropanal by tautomerism [33]. However, these species were not detected in our analysis since they are very reactive. They readily undergo secondary dehydration into acrolein [51,53], the observed product. Furthermore, 3-hydroxypropanal can cleave the C_1—C_2 bond leading to the formation of formaldehyde and acetaldehyde, through retro-aldol reaction. In the presence of oxygen, the generated compounds were oxidized. That is, formaldehyde and acetaldehyde were rapidly oxidized to formic acid and acetic acid, respectively, while acrolein was oxidized to acrylic acid. This resulted in opposite trends in the variation of acrolein and acrylic acid yields, while the yield of acetic acid, glycolic acid and formic acid increased with reaction time as demonstrated in Fig. 6.

4. Conclusions

The use of Al_2O_3-supported POM catalysts in a one-pot process for the liquid phase conversion of glycerol to acrylic acid was successfully performed in liquid phase at low temperature (90 °C). The acid strength of Al_2O_3-supported POM catalysts played an importance role on the conversion and product yield of the oxydehydration of glycerol. The acid strengths of Al_2O_3-supported POM catalysts were in the order of $PW/Al_2O_3 > SiW/Al_2O_3 > PMo/Al_2O_3$, while their oxidative abilities were in the order of $SiW/Al_2O_3 > PW/Al_2O_3 > PMo/Al_2O_3$. The

catalytic activity for oxydehydration of glycerol ranged in the order of $SiW/Al_2O_3 > PW/Al_2O_3 > PMo/Al_2O_3$, suggesting that the oxydehydration of glycerol required the weak–strength acid catalyst and high oxidative ability. Increasing the catalyst loading from 2 to 4 wt.% had a positive effect on the glycerol conversion and product yield. However, at catalyst loading of 8 wt.%, no further improvement in glycerol conversion and product yield was possible due to the lack of oxidizing agent and the onset of mass transfer limitations. Further work will aim at increasing the yield of acrylic acid, by increasing the surface acidity of the catalyst as well as the test of catalytic stability and will be reported in the future.

Acknowledgments

The authors would like to thank the Royal Golden Jubilee (RGJ) Ph.D. Program and the Thailand Research Fund (TRF) for financial support and the Center of Excellence on Petrochemical and Materials Technology (PETRO-MAT), Chulalongkorn University and the Department of Chemical Engineering, Mahanakorn University of Technology for facility support.

References

[1] T. Miyazawa, S. Koso, K. Kunimori, K. Tomishige, Appl. Catal. A 329 (2007) 30–35.
[2] M.J. Taherzadeh, L. Adler, G. Lidén, Enzyme Microb. Technol. 31 (2002) 53–66.
[3] Z. Wang, J. Zhuge, H. Fang, B.A. Prior, Biotechnol. Adv. 19 (2001) 201–223.
[4] M. Hájek, F. Skopal, Bioresour. Technol. 101 (2010) 3242–3245.
[5] W.D. Deckwer, FEMS Microbiol. Rev. 16 (1995) 143–149.
[6] L. Huang, Y. Zhu, H. Zheng, G. Ding, Y. Li, Catal. Lett. 131 (2009) 312–320.
[7] S. Van de Vyver, E. D'Hondt, B.F. Sels, P.A. Jacobs, Stud. Surf. Sci. Catal. 175 (2010) 771–774.
[8] L. Gong, Y. Lu, Y. Ding, R. Lin, J. Li, W. Dong, T. Wang, W. Chen, Appl. Catal. A 390 (2010) 119–126.
[9] S. Kongjao, S. Damronglerd, M. Hunsom, J. Appl. Electrochem. 41 (2011) 215–222.
[10] S.H. Lee, D.J. Moon, Catal. Today 174 (2011) 10–16.
[11] D.A. Simonetti, E.L. Kunkes, J.A. Dumesic, J. Catal. 247 (2007) 298–306.
[12] G. Sabourin-Provost, P.C. Hallenbeck, Bioresour. Technol. 100 (2009) 3513–3517.
[13] E.L. Kunkes, D.A. Simonetti, J.A. Dumesic, W.D. Pyrz, L.E. Murillo, J.G. Chen, D.J. Buttrey, J. Catal. 200 (2008) 164–177.
[14] S.A. Markov, J. Averitt, B. Waldron, Int. J. Hydrogen Energy 36 (2011) 262–266.
[15] D. Ghosh, I.F. Sobro, P.C. Hallenbeck, Bioresour. Technol. 106 (2012) 154–160.
[16] A. Chieregato, F. Basile, P. Concepción, S. Guidetti, G. Liosi, M.D. Soriano, C. Trevisanut, F. Cavani, J.M.L. Nieto, Catal. Today 197 (2012) 58–65.
[17] L. Shen, H. Yin, A. Wang, Y. Feng, Y. Shen, Z. Wu, T. Jiang, Chem. Eng. J. 180 (2012) 277–283.
[18] C.A. Henao, D. Simonetti, J.A. Dumesic, C.T. Maravelias, Comput. Aided Chem. Eng. 27 (2009) 1719–1724.
[19] F. Li, F. Xue, B. Chen, Z. Huang, Y. Yuan, G. Yuan, Appl. Catal. A 449 (2012) 163–171.
[20] Z.Y. Zakaria, J. Linnekoski, N.A.S. Amin, Chem. Eng. J. 207–208 (2012) 803–813.
[21] C. Beatrice, G.D. Blasio, M. Lazzaro, C. Cannilla, G. Bonura, F. Frusteri, F. Asdrubali, G. Baldinelli, A. Presciutti, F. Fantozzi, G. Bidini, P. Bartocci, Appl. Energy 102 (2013) 63–71.
[22] V.C. Malshe, S.B. Chandalia, J. Appl. Biotechnol. Chem. 27 (5) (1977) 575–584.
[23] J. Tichý, Catal. Appl. A 157 (1997) 363–385.
[24] J. Kunert, A. Drochner, J. Ott, H. Vogel, H. Fue, Catal. Appl. A 269 (2004) 53–61.
[25] P. Kampe, L. Giebeler, D. Samuelis, J. Kunert, A. Drochner, F. Haa, A.H. Adams, J. Ott, S. Endres, G. Schimanke, T. Buhrmester, M. Martin, H.F.H. Vogel, Phys. Chem. 9 (2007) 3577–3589.
[26] J. Xu, J.-L. Dubois, W. Ueda, ChemSusChem 3 (2010) 1383–1389.
[27] F. Wang, J.-L. Dubois, W. Ueda, J. Catal. 268 (2009) 260–267.
[28] F. Wang, J.-L. Dubois, W. Ueda, Appl. Catal. A 376 (2010) 25–32.
[29] J. Deleplanque, J.-L. Dubois, J.-F. Devaux, W. Ueda, Catal. Today 157 (2010) 351–358.
[30] M.D. Soriano, P. Concepció, J.M.L. Nieto, F. Cavani, S. Guidettiand, C. Trevisanut, Green Chem. 13 (2011) 2954–2962.
[31] A. Witsuthammakul, T. Sooknoi, Appl. Catal. A 413–414 (2012) 109–116.
[32] A. Popa, V. Sasca, E.E. Kis, R.M. Neducin, M.T. Bokorov, J. Halasz, J. Optoelectron. Adv. Mater. 7 (2005) 3169.
[33] E. Tsukuda, S. Sato, R. Takahashi, T. Sodesawa, Catal. Commun. 8 (2007) 1349–1353.
[34] M.T. Pope, Heteropoly and Isopoly Oxometalates, Springer-Verlag, Berlin, 1983.
[35] P. Stati, S. Freni, S. Hocevar, J. Power Sources 79 (1999) 250.
[36] D.P. Padiyan, S.J. Ethilton, K. Paulraj, Cryst. Res. Technol. 35 (2000) 87–90.
[37] F. Babou, G. Coudurier, J.C. Vedrine, J. Catal. 152 (1995) 341–349.
[38] J.M. Tatibouët, C. Montalescot, K. Brückman, Appl. Catal. A 138 (1996) L1–L6.
[39] C.R. Deltcheff, M. Fournier, R. Franck, R. Thouvenot, Inorg. Chem. 22 (1983) 207–216.
[40] U.L. Stangar, N. Grošelj, B. Orel, Ph. Colomban, Chem. Mater. 12 (2000) 3745–3753.
[41] H.J. Kim, Y.G. Shul, H. Han, Appl. Catal. A 299 (2006) 46–51.
[42] S. Uchida, K. Inumaru, M. Misono, J. Phys. Chem. B 104 (2000) 8108–8115.
[43] I.V. Kozhevnikov, Chem. Rev. 98 (1998) 171–198.
[44] S. Damyanova, J.L.G. Fierro, I. Sobrados, J. Sanz, Langmuir 15 (1999) 469–476.
[45] G.R. Rao, T. Rajkumar, B. Varghese, Solid State Sci. 11 (2009) 36–42.
[46] R. Thouvenot, C. Rocchiccioli-Deltcheff, M. Fournier, J. Chem. Soc. Chem. Commun. (1991) 1352–1354.
[47] B. Pawelec, S. Damyanova, R. Mariscal, J.L.G. Fierro, I. Sobrados, J. Sanz, L. Petrov, J. Catal. 223 (2004) 86–97.
[48] K.M. Delak, T.C. Farrar, N. Sahai, J. Non-Cryst. Solids 351 (2005) 2244–2250.
[49] H. Atia, U. Armbruster, A. Martin, J. Catal. 284 (2008) 247–258.
[50] B.B. Bardin, S.V. Bordawekar, M. Neurock, R.J. Davis, J. Phys. Chem. B 102 (1998) 10817–10825.
[51] W. Suprun, M. Lutecki, T. Haber, H. Papp, J. Mol. Catal. A: Chem. 309 (2009) 71–78.
[52] E.G. Rodrigues, M.F.R. Pereira, J.J. Delgado, X. Chen, J.J.M. Órfão, Catal. Commun. 16 (2011) 64–69.
[53] W. Yan, G.J. Suppes, Ind. Eng. Chem. Res. 48 (2009) 3279–3283.